DENTAL MATERIALS 35 (2019) 1614–1629

Available online at www.sciencedirect.com

ScienceDirect

journal homepage: www.intl.elsevierhealth.com/journals/dema

# The synthesis of nano silver-graphene oxide system and its efficacy against endodontic biofilms using a novel tooth model*

*Konstantinos Ioannidis*[a], *Sadia Niazi*[b], *Petros Mylonas*[a], *Francesco Mannocci*[a], *Sanjukta Deb*[a,*]

[a] *Centre for Oral Clinical & Translational Science, Faculty of Dentistry, Oral & Craniofacial Sciences, Floor 17, Tower Wing, Guy's Hospital, London Bridge, King's College London, London SE1 9RT, UK*

[b] *Department of Endodontics, Faculty of Dentistry, Oral & Craniofacial Sciences, Postgraduate Centre, Floor 22, Tower Wing, Guy's Hospital, London Bridge, King's College London, London SE1 9RT, UK*

ARTICLE INFO

*Article history:*
Accepted 22 August 2019

*Keywords:*
Biofilm
Endodontics
Graphene oxide
Irrigation
Root canal
Silver nanoparticles
Ultrasonics

ABSTRACT

*Objective.* The deleterious caustic effects of sodium hypochlorite (NaOCl) as a root canal irrigant makes it imperative that alternative methods are developed for root canal disinfection. The purpose of this study was to examine the antimicrobial efficacy of silver nanoparticles (AgNPs) synthesized on an aqueous graphene oxide (GO) matrix (Ag-GO), with different irrigant delivery methods to enhance the disinfection regimen, using a novel *ex vivo* infected tooth model.

*Methods.* AgNPs were prepared by reducing $AgNO_3$ with 0.01 M $NaBH_4$ in presence of GO. Elemental analysis was performed with scanning electron microscopy/energy dispersive X-ray spectroscopy (SEM/EDS) and scanning transmission electron microscopy (STEM) was used for size and morphology analysis of GO and Ag-GO. Nutrient stressed, multi-species biofilms were grown in prepared root canals of single-rooted teeth. The irrigants used were sterile saline, 1% and 2.5% NaOCl, 2% chlorhexidine gluconate (CHX), 17% EDTA and an aqueous suspension of 0.25% Ag-GO. The antimicrobial efficacy of the irrigants were performed with paper point sampling and measurement of microbial counts. The biofilm disruption in dentine tubule surfaces was analysed with confocal laser scanning microscopy (CLSM). The acquisition of total biovolume ($\mu m^3/\mu m^2$) and biofilm viability was performed using software BioImage_L. Two-way analysis of variance (ANOVA) with post hoc Tukey tests was used for data analysis with level of statistical significance set at $P < 0.05$.

*Results.* SEM/EDS analysis confirmed impregnation of Ag within the GO matrix. TEM images showed polygonal GO sheets and spherical AgNPs of diameter 20–50 nm, forming a network on the surface of GO sheets. The use of ultrasonic activation enhanced the efficacy of Ag-GO compared to 1% NaOCl, 2% CHX, 17% EDTA and sterile saline ($P < 0.05$). The microbial killing efficacy of 2.5% NaOCl was superior compared to the experimental groups. The maximum biofilm disruption, in dentine tubule surfaces, was achieved by 2.5% NaOCl, however Ag-GO caused a significant reduction of total biovolumes compared to the rest of the experimental groups ($P < 0.05\%$).

* This research did not receive any specific grant from funding agencies in the public, commercial, or not-for-profit sectors.

* *Corresponding author.*
E-mail address: sanjukta.deb@kcl.ac.uk (S. Deb).

https://doi.org/10.1016/j.dental.2019.08.105

*Significance.* The successful documentation of the microbial killing and biofilm disruption capacity of Ag-GO is a promising step forward to explore its unique properties in clinical applications and biomaterials in dentistry.



## 1. Introduction

Infections in the dental root canal are biofilm mediated [1]. The properties of bacteria that inhabit a biofilm are different from those of planktonic cells, since bacterial congregations possess higher resistance to antimicrobial agents [1]. Bacterial growth within a necrotic root canal is the main cause of apical periodontitis [2,3]. Mechanical debridement and chemical irrigation with sodium hypochlorite (NaOCl) solution, often, is not enough to rid the root canal off bacteria. These tend to adapt within stressed micro-environmental conditions usually in the form of a biofilm [4,5]. The use of mechanical instrumentation to clean the root canal is successful to an extent, however large areas of the canal remain un-instrumented, potentially leaving substantial areas of biofilm along with necrotic tissue remnants [6]. Persistent infection in such confined areas is regarded as a common cause of root canal treatment failure and post-treatment apical periodontitis [7–9].

Sodium hypochlorite (NaOCl) (1–5%) is currently regarded as a gold standard for irrigation and chemical disinfection of the root canal system due to its antimicrobial effects, ability to disintegrate, solubilize organic tissue and denature toxins [10–13]. However, the irrigant needs to reach and disrupt the biofilm matrix even in less accessible areas of the root canal system [14], hence several agitation and activation methods have been proposed to improve efficacy, including sonic & ultrasonic activation, negative apical pressure irrigation, laser activation and physical agitation using XP Endo Finisher (XPEF) (FKG Dentaire, Switzerland) [15,16].

NaOCl is known for its deleterious effects against dentine collagen [17] and its caustic effects on soft and hard tissues [18,19]. In addition, when NaOCl reacts with compounds of the infected root canal, toxic volatile compounds and chlorinated disinfection by-products are also formed [20,21]. Other agents that are used as irrigants in endodontics include chlorhexidine 2% (CHX) and ethylenediamine tetra-acetic acid 17% (EDTA), however the ability to totally disrupt biofilms remain questionable [22,23].

The incorporation of nanoparticles (NPs) into disinfection strategies has gained attention in the past few decades due to their innovative and functional properties. Antibiotic resistance and prevalence of biofilms are major threats, which has triggered the exploration of alternative approaches to minimise the burden of drug-resistant microbial infections [24]. Nanoparticles of silver (Ag NPs) have been reported to promote antibacterial activity compared to conventional silver-based materials [25,26].

Graphene oxide (GO) is chemically exfoliated from oxidized graphite that constitutes monolayers of carbon nano-sheets forming dense honeycomb structures [27] with hydroxyl and epoxide functional groups on the two sides and carboxylic groups at the edges [28,29]. GO exhibits antibacterial activity against several bacterial species [30,31] and is considered as a promising material for biological applications [29,32]. Recent studies have shown that the use of a layered material such as GO as a matrix can compensate for the lack of stability and aggregation of sole Ag NPs dispersions, leading to high binding capability and enhanced, synergistic antimicrobial action [33,34].

This study reports the synthesis of Ag NPs on GO particles (Ag-GO) with the antimicrobial and biofilm disruption ability of Ag-GO particles compared to sterile saline, EDTA 17%, CHX 2%, NaOCl 1% and 2.5%, with conventional irrigation (CI), ultrasonically activated irrigation (UAI) and XP Endo Finisher (XPEF). A newly proposed infected tooth model was used to validate the *in vitro* findings.

## 2. Materials and methods

### 2.1. Specimen selection and preparation

Freshy extracted single rooted teeth with a single canal, free of cracks, fractures, caries, abrasions and discolouration were collected, in accordance with the protocol outlined in the Research Ethical Committee Document (Wales REC 4, 14/WA/1004, UK). For a number of 20 groups, total sample size was calculated 120 (n = 6 per group) with G*Power 3.1.9.2 software (Franz Faul, Universitaet Kiel, Germany) with an a-value of 0.05, an actual power of 80% and an effect size (f) of 0.23 (partial $\eta^2 = 0.05$).

All specimens were initially autoclaved at 121 °C for 15 min. The crowns of teeth were removed and the root length was standardised to 15 mm. Root canals were accessed and scouted with K-files size 10 (Dentsply Sirona, Ballaigues, Switzerland) to ensure patency until their tip was detected through apical foramen, under magnification with an operating dental microscope (Global, USA). The working length was established by subtracting 0.5 mm. The root canals were prepared with ProTaper Universal (Dentsply Sirona, Switzerland) rotary files up to F3 instrument (apical diameter 0.30 mm, taper 0.09). Irrigation was performed with NaOCl 5.25% (Chloraxid, Cerkamed, PL) using a total volume of 8 ml (2 ml per file sequence). EDTA 17% (Schottlander & Davis, UK) (2 ml) was used to remove the inorganic phase of the smear layer. Root canals were finally flushed with 2 ml distilled water and dried with sterile paper points.

Each tooth was longitudinally hemi sectioned in a buccolabial orientation with a wafering blade [35]. The specimen half with the most conserved root canal was used for the preparation of two artificial lateral canals using a cylindrical diamond bur with 0.25 mm radius (111-010M pk5, Dentsply, Switzerland), under magnification with an operating dental

microscope (Global, USA). The lateral canals were prepared in the apical (3 mm from root apex) (LAT1) and middle third (6 mm from root apex) (LAT2). These specimens were selected for the biofilm growth.

### 2.2. Artificial lateral canal characterisation

To ensure standardisation in the creation of artificial lateral canals and thus homogeneity in lateral canal dimensions in all samples entered into the study, 7% of the samples (n = 8) were randomly selected and digitally scanned using non-contacting laser profilometry (NCLP) (XYRIS 4000CL, Taicaan Technologies, UK). The NCLP had a 2 μm spot size, with dimensional accuracy 10 nm (z), <1 μm (x, y) and reproducibility accuracy 238 nm. Lateral canals were scanned with scanning x (width), y (length) dimension 3.5 × 1.5 mm using a 10 μm step over, producing digital point-cloud data of 53,001 individually measured points per lateral canal [36]. Laterals canals were then dimensionally analysed for their mean x, y dimensions (mm) using automated in-software digital callipers, whilst mean z (depth) dimension (mm) was measured using 3-D step height according to ISO 5436-1 [36]. Dimensional analysis was calculated using a bespoke automated macro written to allow objective analysis of all digital data sets using specialist metrology software (MountainsMap, Digital Surf, France). The process of lateral canal scanning, digitisation, and lateral canal dimensional analysis is summarised in Fig. 1.

### 2.3. Fabrication of testing apparatus

A novel testing apparatus was fabricated to simulate the conditions of intracanal irrigation, with the use of an *ex vivo* closed apical system, to reflect periapical tissue resistance to irrigant extrusion [37]. Prior to hemi sectioning, each root specimen was vertically stabilised on its coronal surface with thermoplasticised silicon glue. A zinc plated mini fuel hose line pipe clip (diameter: 11–13 mm, height: 10 mm) (Wilson Lendrum & Weir, UK) was positioned in the periphery of the root specimen to achieve a centring position of specimen within the diameter of the clamp margins. The clamp was then filled with injectable thermo-plasticised silicon glue with the aid of a glue gun (Bosch PKP 18 E, Robert Bosch Holdings, UK) (Fig. 2a). The root specimen was covered up to apical third by silicon glue which was cylindrically shaped after application of vertical pressure with the aid of a 3-ml clear glass bottle (Ampulla, Cheshire, UK) (Fig. 2b). A polyvinylsiloxane silicon (Aquasil, Dentsply DeTrey, Konstanz, Germany) key impression was taken for the apical root segment and the cylindrical silicone index to ensure apical seal and to simulate apical tissue resistance (Fig. 2c).

After the hemi section of the specimens, the split halves (Fig. 2d & e) were re-approximated within the apparatus and further merged into the apical silicon index. The clamp was tightened with the aid of an electric screwdriver (Bosch IXO, Robert Bosch Holdings, UK), to ensure the performance of the apparatus as a single unit (Fig. 2f–h). Prior to use, the testing apparatus was sterilised under UV to reduce risk of cross-infection during the experimental procedures. To ensure that all geometrical aspects were exposed to UV light, the apparatus was frequently repositioned every 20–30 min, to ensure most surfaces were exposed.

### 2.4. Development of multispecies stressed biofilm in hemi-sectioned root halves

One hundred and fourteen pairs of root halves (n = 114) were randomly assigned to 1 positive control (biofilm growth/no treatment) and 18 treatment groups. Each of the 19 groups included six pairs of root halves. Six additional pairs of autoclaved, sterile root halves served as negative control group (no biofilm growth).

A stressed multispecies biofilm comprising of five selected bacteria was developed on the root canal of each selected hemi section using the protocol developed by Niazi et al. [35]. The selected endodontic bacteria in this biofilm included *Propionibacterium acnes*, *Actinomyces radicidentis*, *Staphylococcus epidermidis*, *Streptococcus mitis* -recovered from root canals of teeth with refractory endodontic infections- and *Enterococcus faecalis* strain OMGS 3202 [38,39].

To establish biofilms, the strains were cultured anaerobically at 37 °C for seven days on Fastidious Anaerobe Agar (FAA) supplemented with 5% defibrinated horse blood (FAA, Thermo Scientific™, UK), suspended in modified fluid universal medium (mFUM) [40] and incubated at 37 °C for 3 h in anaerobic workstation (MACS-MG-1000, Don Whitley Scientific Ltd, UK). The absorbance was adjusted to 0.5 at 540 nm to obtain $10^7$ cells/ml (Labsystems iEMS Reader MF, Basingstoke, UK) [35].

The selected root halves were autoclaved at 121 °C for 15 min and placed with the aid of sterile tweezers in sterile 24-well plates (CytoOne®, Starlab, UK). Two ml of mFUM were added and the specimens were initially pre-reduced in an anaerobic atmosphere (80% nitrogen, 10% hydrogen and 10% carbon dioxide) for 2 h. After this period, the mFUM was aspirated and each root half was further seeded with 400 μl of each of the five starter cultures. The biofilms were grown anaerobically with regular medium change after every 24 h for the first 7 days and the biofilms were left to grow for the next 7 days in the unchanged medium in order to stress the microorganisms nutritionally [35].

### 2.5. Synthesis and characterisation of Ag NPs in GO aqueous solution (Ag-GO)

A GO aqueous dispersion (10 mg/ml) (GoGraphene, William-Blythe, Harlow, UK) was used and the dispersion was progressively diluted in sterile distilled water to a lower concentration below 6 mg/ml to ensure transition from pseudoelastic fluid to Newton fluid state [41]. To ensure effective syringe delivery with the aid of open-ended irrigation needle (27-G), the solution was finally diluted to 2.5 mg/ml.

Ag NPs were prepared by reducing $AgNO_3$ with $NaBH_4$ in presence of GO suspension, according to the method by Das et al. [33]. Typically, 10 ml of homogeneous suspension of GO (2.5 mg/ml) was mixed with 10 ml aqueous $AgNO_3$ solution 0.01 M (Sigma-Aldrich, Gillingham, UK) and the reaction mixture was stirred for 30 min at room temperature, before the addition of the reducing agent. Subsequently, 1 ml of a freshly prepared solution of $NaBH_4$ 0.01 M (Sigma-Aldrich,

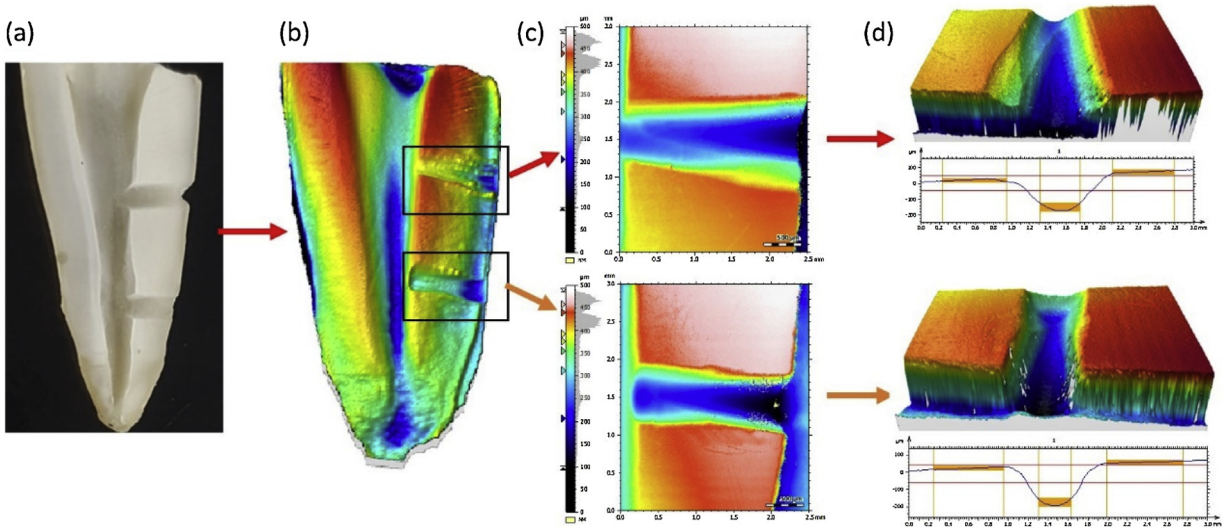


**Fig. 1 – Artificial lateral canal characterisation. (a) Hemisected tooth model specimen. (b) Tooth model digitised using non-contacting laser profilometry. (c) Lateral canal dimensional analysis. (d) Automated dimensional analysis, x,y dimensions using digital calipers and z dimension using 3D step height analysis according to ISO 5436-1. The relevant data were expressed as mean (SD) 3D step height (mm).**

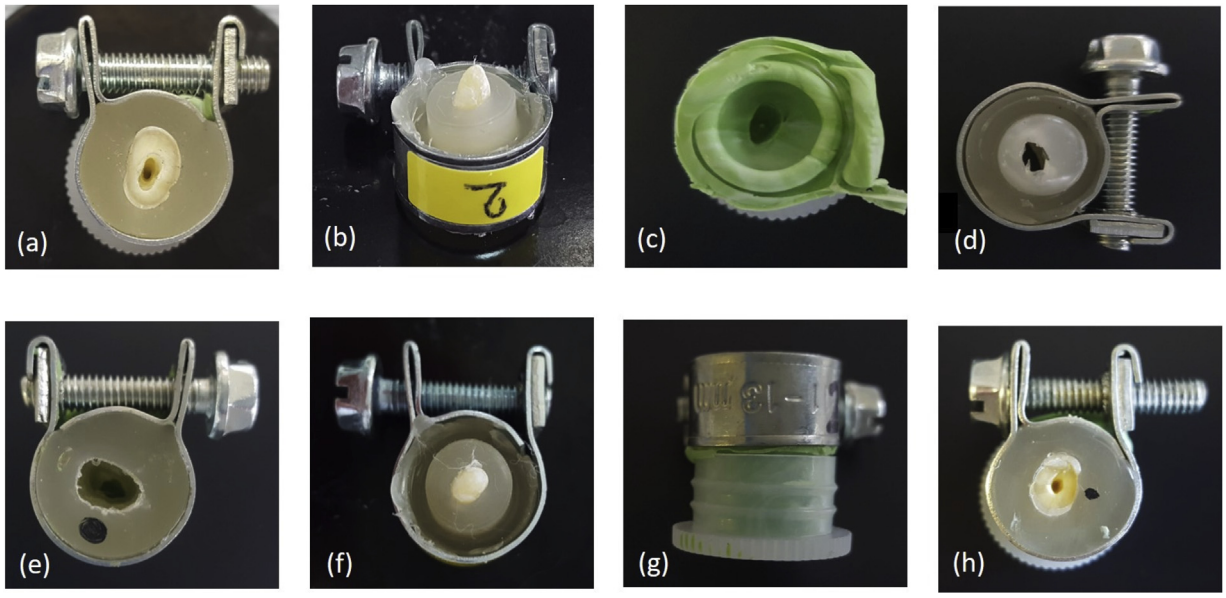


**Fig. 2 – Infected tooth-model testing apparatus. (a) Coronal view of clamp-silicon index. (b) Apical view of clamp-silicon index. (c) Silicon key-impression of apical root segment. (d, e) Removal of root specimen and inspection of silicon internal surfaces to ensure absence of structural deficiencies after setting. (f, g, h) Re-assembling of hemisected root specimens, addition of silicon key to simulate apical pressure resistance and tightening of the clamp.**

Gillingham, UK) was added slowly to the reaction mixture of $AgNO_3$–GO suspension with vigorous stirring. The colour of the reaction mixture turned into dark brown to grey. The reaction mixture was stirred for another 5 h for complete reduction at room temperature. The Ag-GO nanoparticles were typically used within 24–48 h of preparation and stored in a refrigerator. No stability studies on these particles were carried out in this study, however agglomeration of particles may occur on long term storage in physiological solutions.

For elemental analysis of Ag-GO, scanning electron microscopy/energy dispersive X-ray spectroscopy (SEM/EDS) (NeoScope JCM-6000plus, Japan) at 10 kV was used to confirm the impregnation of Ag NPs in GO matrix. One millilitre (1 ml) of Ag-GO suspension was left to air-dry and the solid sheets were placed on 12.5 mm aluminium pin stubs (Agar Scientific Elektron Technology UK, Stansted, UK) using Leit C conducting carbon cement (Agar Scientific Elektron Technology UK, Stansted, UK) and gold- or carbon-coated for SEM or

EDS imaging, respectively. The sizes and morphologies of GO and Ag-GO were characterized by scanning transmission electron microscopy (STEM) (JEOL JEM-F200 microscope, Japan) at 200 kV.

### 2.6. Protocols of irrigation procedures

The irrigants tested in experimental groups were: Sterile saline (NaCl 0.9%) (JFA Medical, Blackpool, UK), EDTA 17% (Schottlander & Davis, UK) NaOCl 1%, NaOCl 2.5%, chlorhexidine 2% (CHX) (GlucoChex, Cerkamed, PL) and Ag-GO (2.5 mg/ml). Concentrated NaOCl solutions were prepared from a stock solution NaOCl ≥10% (Sigma Aldrich, Gillingham, UK) and verified with iodometric titration [42]. After NaOCl irrigation, the root canals were washed with 1 ml sodium thiosulphate ($Na_2SO_4$) 0.1 M (Sigma Aldrich, Gillingham, UK) to neutralise any residual chlorine activity.

Three types of irrigation procedures were used: Conventional irrigation (CI), ultrasonically activated irrigation (UAI) and irrigation with application of XP Endo Finisher (XPEF). The performance of the respective irrigation and agitation procedures is summarised in Fig. 3(a–c).

Syringe irrigation was performed using a 27-G open-ended needle and a 3 ml-containing syringe with a luer-lock (Monoject, Medtronic, UK). A rubber-stop was applied 3 mm short of working length. Irrigation was carried out by an accredited Specialist Endodontist using digital pressure with the forefinger only at a rate compatible with the time stated for each irrigation procedure. The needle was moved up and down in the canal gently, ensuring that it did not bind on axial walls.

Ultrasonically activated irrigation was conducted with a size 25 ultrasonic file with zero taper (Irrisafe, Acteon, UK) placed in the canal, filled with each irrigant type. The ultrasonic unit (Newtron Booster, Acteon, UK) was adjusted for endodontic use (ring colour at yellow) with a power setting at 9, according to the manufacturer's recommendations. The file was inserted into the canal 1 mm short of working length. File oscillation was performed towards the lateral canals' direction with no constraint.

The XP Endo Finisher file was inserted vertically in gentle longitudinal vertical motion of 7–8 mm against the sidewalls of the canals. The insertion depth was 1 mm short of the working length and it was operated according to the manufacturer's instructions, with a motor rate of 800 rpm and torque 1 Ncm. To ensure file efficacy, each allocated tooth specimen

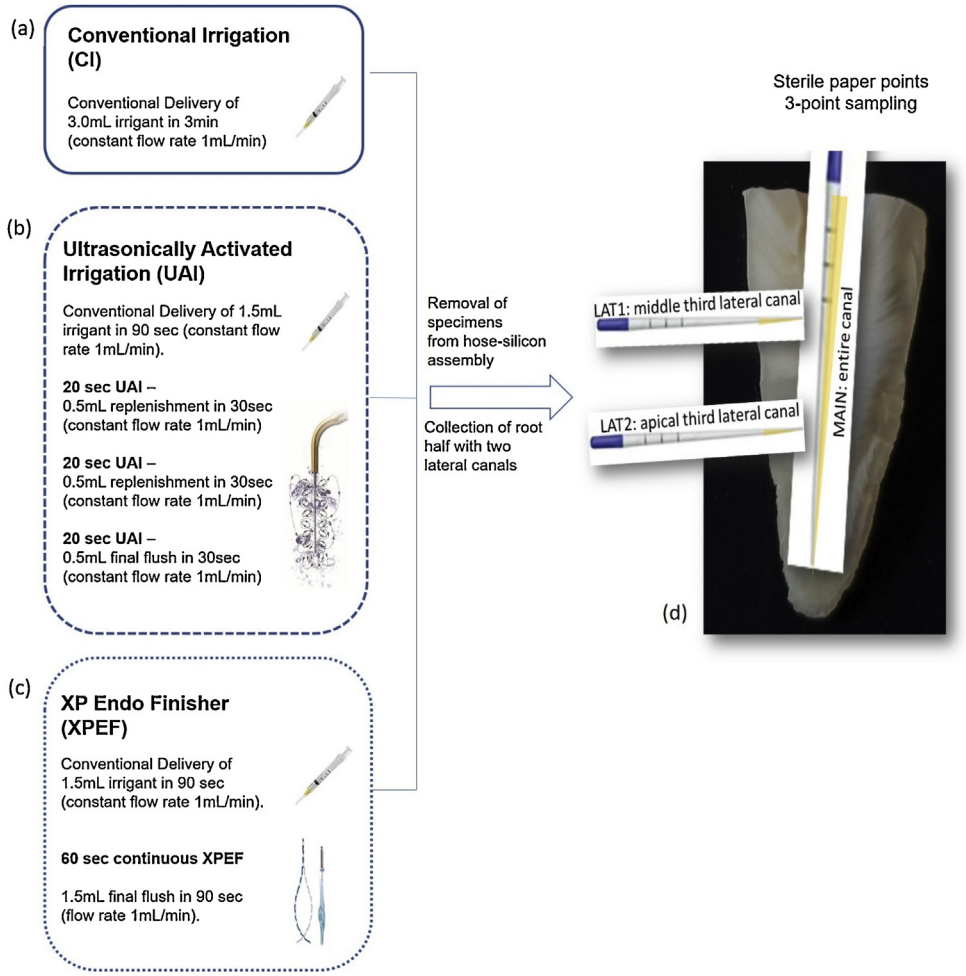


**Fig. 3 – Protocols of irrigation procedures and 3-point sampling areas. (a) Conventional irrigation (CI). (b) Ultrasonically Activated Irrigation (UAI). (c) Application of Endo XP Endo Finisher (XPEF). (d) 3-point paper point sampling areas including main canal lumen (MAIN), middle root third lateral canal (LAT1) and apical root third lateral canal (LAT2).**

was treated immediately after removal from 37 °C anaerobic incubation.

### 2.7. Determination of quantitative viable counts of the biofilms after irrigation

Once irrigation procedures were complete, the clamp of the silicon-fused hose was untightened, the apical silicon index was removed, the merged root fragments were simultaneously taken out of the apparatus and the chosen root half with the two lateral canals was placed in a 9-cm sterile Petri dish (SLS, Nottingham, UK). For the quantitative measurement of the microbial viable counts, 3-point sampling (MAIN: entire canal; LAT1: middle third lateral canal; LAT2: apical third lateral canal) was performed using sterile paper points (Protaper Universal F3 Paper point, Dentsply Sirona, Switzerland) (Fig. 3d). Sampling in the main canal was performed by soaking a paper point within the length of the canal lumen for 30 s. Sampling in the lateral canals was performed by inserting the paper point tips only within their dimensions for 30 s.

The sampled paper points were dispersed into 1 ml of BHI (Brain–Heart infusion Broth, Lab M) and vortexed for 2 min. After serial dilution in BHI, aliquots (100 μl) were plated onto duplicate FAA plates and incubated anaerobically at 37 °C for 7 days. After the incubation period, the numbers of colonies and their $\log_{10}$ ($\log_{10}$CFU) were counted.

### 2.8. Confocal laser scanning microscopy (CLSM) analysis of the multispecies biofilm

After sampling for quantitative viable counts, the biofilms of 3 specimens per group were stained with a Live/Dead Baclight bacterial viability kit (Thermofisher Scientific, UK). This kit is used to assess the viability of bacterial populations as a function of the membrane integrity of the cell. In this study, it was used as an indicator or surrogate measure of microbial cell viability, following disinfection procedures. Cells with a compromised membrane that are considered to be dead or dying will stain red, whereas cells with an intact membrane will stain green.

An inverted Leica TCS SP2 confocal laser scanning microscope (Leica Microsystems, Milton Keynes, UK) was used. The specimens were transferred into 35-mm cell imaging coverglass-bottom dishes (SPL LifeSciences, Korea), with their root canal surface facing the bottom of the dish towards the objective. A ×63 magnification oil immersion objective with a numerical aperture of 1.40 and a confocal pinhole to Airy 1 unit was used to observe the fluorescence emission of SYTO® 9 and Propidium Iodide using 488 nm and 569 nm (Ar-Kr laser) as the excitation source, respectively. Image acquisition was performed with a zoom factor of 4.0, a pixel resolution of 0.11 μm/pixel and field resolution of 512 × 512 pixels. Three z-stacks were acquired from each root specimens: apical third of the main canal, middle lateral canal and apical lateral canal. Each stack had a substratum coverage field area of 59.52 μm × 59.52 μm. For each stack, the z-step for the images was 2 μm and 10 2-D images were acquired.

The acquired images of all biofilms in each group were analysed using bioImage_L [43]. This novel image analysis software package was designed to calculate biofilm structural parameters in oral biofilms stained with dual-channel fluorescent markers [43]. It applies an *in situ* colour segmentation routine that automatically segments the colour image into individual pseudochannels, and the areas and percentages of each identified colour subpopulation are calculated and presented. By identifying colour tonalities *in situ*, the software independently processes the colour subpopulations and characterises the viability and metabolic activity of biofilms [43].

Biofilm disruption was expressed by mean [standard error(se)] values of total biovolumes ($\mu m^3/\mu m^2$) and % percentages of dead (red), live (green) and unknown (orange) populations within residual biofilms, obtained by bioImage_L analysis. The detection of unknown (orange) populations may result from an intermediate cellular state, in which the partially damaged bacterial membranes can allow the penetration of fluorescing Propidium Iodide, even when the cells are viable [35].

### 2.9. Statistical analysis

Two-way analysis of variance (ANOVA) with post hoc Tukey tests was used for data analysis and comparison of the quantitative viable counts amongst all groups. The overall analysis was performed with SPSS software (version 22.0, IBM SPSS Inc., Chicago, IL, USA). The level of statistical significance was set at $P < 0.05$. The acquisition of total biovolume ($\mu m^3/\mu m^2$) and percentage of biofilm viability (% green/red/unknown) for each group was performed with BioImage_L [43], by performing two-way analysis of variance (ANOVA).

## 3. Results

### 3.1. Artificial lateral canal characterisation

Dimensional analysis revealed that the artificial middle lateral canals mean (SD) x, y, z dimensions were 0.383 (0.057) mm, 2.232 (0.213) mm and 0.256 (0.044) mm, whilst the apical lateral canals mean (SD) x, y, z dimensions were 0.371 (0.061) mm, 1.737 (0.204) mm, 0.216 (0.049) mm. No statistically significant difference ($P > 0.05$) was observed in the dimensions between either type of lateral canal (Table 1).

### 3.2. Characterisation of Ag-GO with SEM/EDS and TEM

SEM/EDS analysis confirmed the presence of Ag and its impregnation within the GO structure (Fig. 4a–c). In addition,

**Table 1 – Mean (SD) length (y), width (x) and depth (z) (mm) are shown for both middle and apical artificial lateral canal.**

| Lateral canal dimensional analysis | | |
|---|---|---|
| | Middle (LAT1) (n = 8) | Apical (LAT2) (n = 8) |
| Mean (SD) Length (y) (mm) | 2.232 (0.213) | 1.737 (0.204) |
| Mean (SD) Width (x) (mm) | 0.383 (0.057) | 0.371 (0.061) |
| Mean (SD) Depth (z) (mm) | 0.256 (0.044) | 0.216 (0.049) |

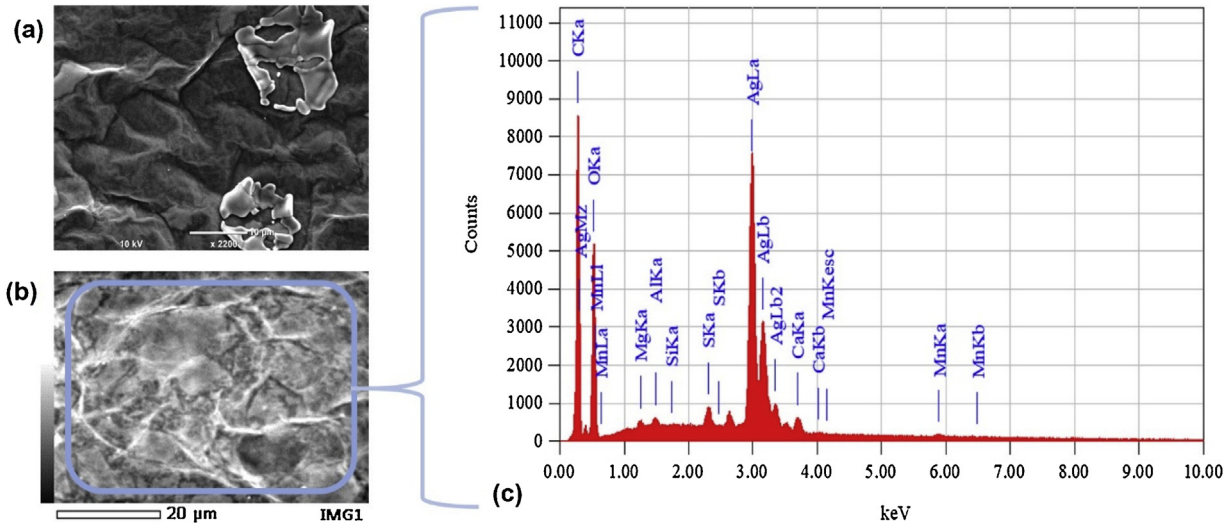


**Fig. 4 – (a) SEM analysis of Ag-GO precipitates in aqueous solution at 10 µm scale and ×2.2k magnification. Silver agglomeration is present. (b, c) Elemental analysis of the sample obtained by EDS.**

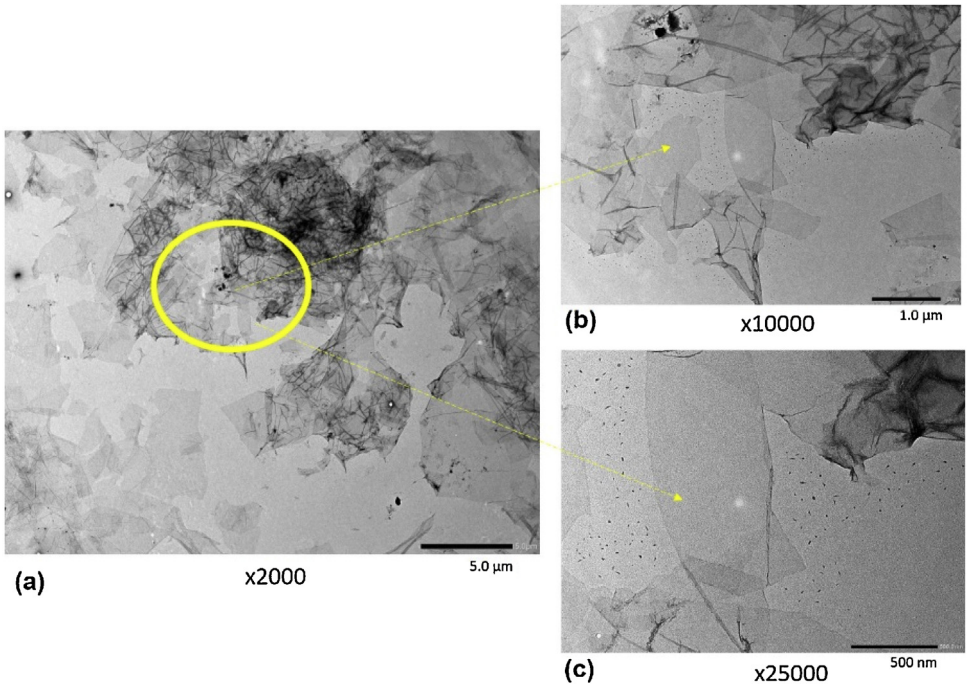


**Fig. 5 – TEM images of graphene oxide at different magnifications and scale bars ((a) ×2000/5 µm, (b) ×10,000/1 µm, (c) ×25,000/500 nm).**

areas of Ag agglomeration were noticeable with diameters varying from 7 to 20 µm (Fig. 4a). The analysis of TEM images confirmed the morphology of polygonal GO sheets (Fig. 5a–c). Ag-GO dispersion contained spherical Ag NPs of diameter 20–50 nm, which were evenly distributed and anchored, on the surface of GO sheets (Fig. 6).

### 3.3. *Effect of irrigants on microbial killing*

#### 3.3.1. *Entire canal sampling point (MAIN)*

NaOCl 2.5% presented the lowest values of detectable viable counts ($log_{10}$CFU) and was significantly more effective in microbial killing than the other irrigants, regardless of irrigant delivery method ($P < 0.05$) (Fig. 7).

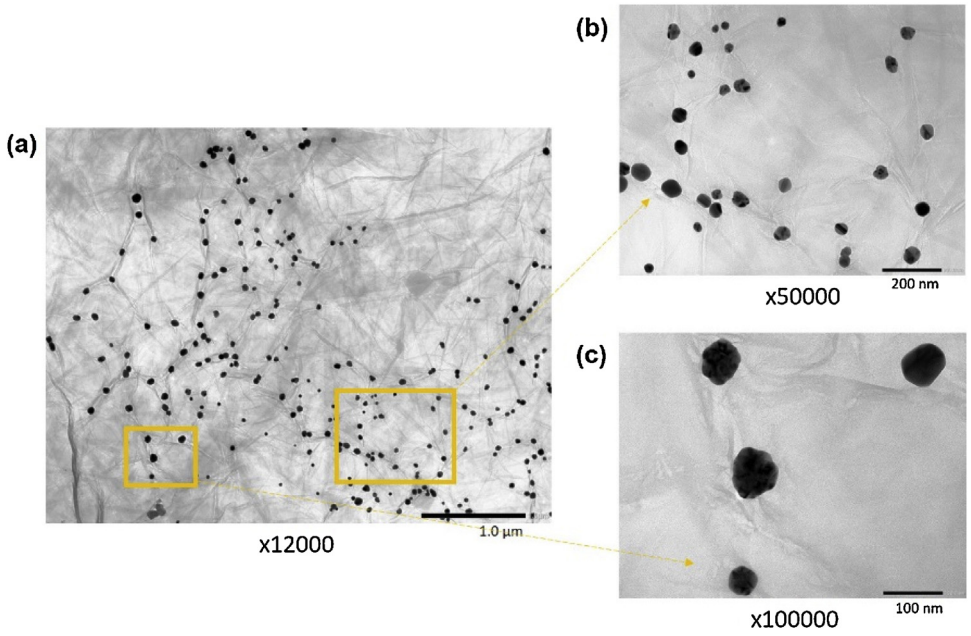


**Fig. 6 – TEM images of Ag nanoparticles on the graphene oxide sheets at different magnifications and scale bars ((a) ×12k/1 µm, (b) ×50k/200 nm, (c) ×100k/100 nm).**

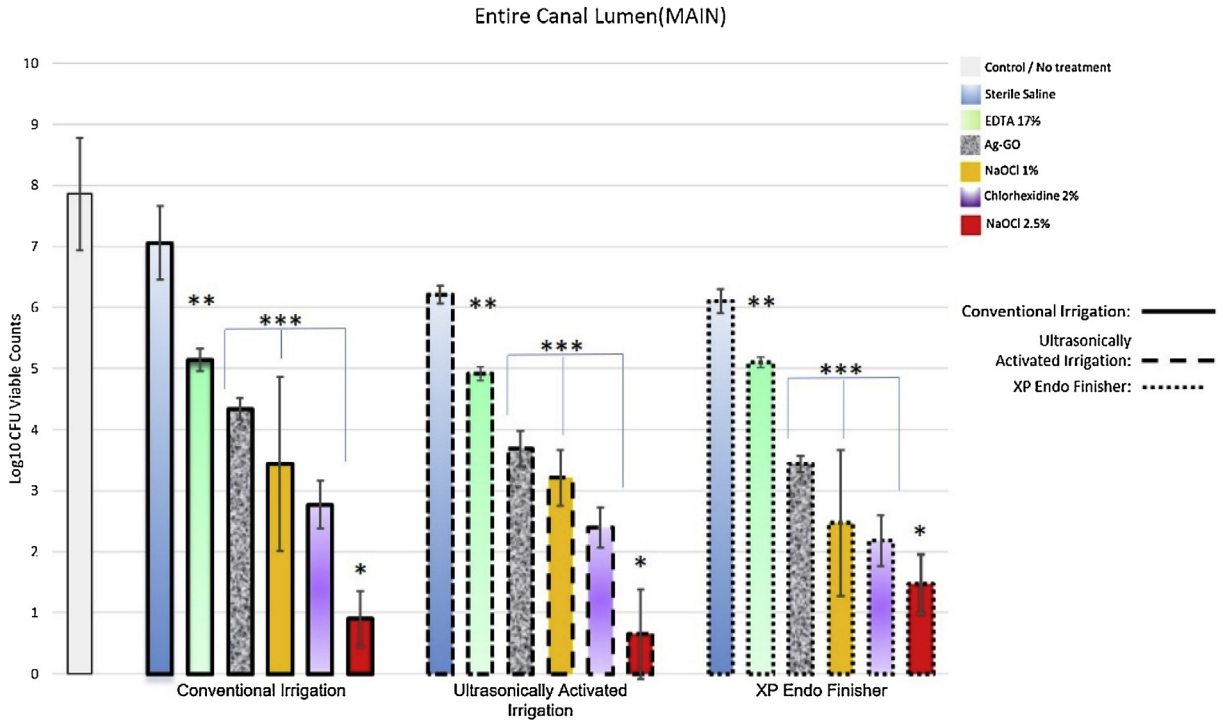


**Fig. 7 – The effect of microbial killing of root canal irrigants and agitation methods in the main canal lumen (MAIN). The data are expressed as mean (SD) detectable anaerobic quantitative viable counts ($log_{10}$CFU).**
***Values significantly less compared to rest experimental groups ($P < 0.05$). ****Values significantly less compared to sterile saline groups ($P < 0.05$). *****Values significantly less compared to EDTA 17% and sterile saline groups ($P < 0.05$) and no statistically significant differences at their inter-group comparisons ($P > 0.05$).**

Ag-GO, NaOCl 1% and CHX 2% presented similar efficacy, which was significantly higher than sterile saline and EDTA 17% ($P < 0.05$) (Fig. 7). The application of UAI or XPEF did not significantly affect the number of detectable viable counts ($log_{10}$CFU) compared to CI ($P > 0.05$) (Fig. 7).

Negative control group specimens presented non-detectable viable counts ($log_{10}$CFU).

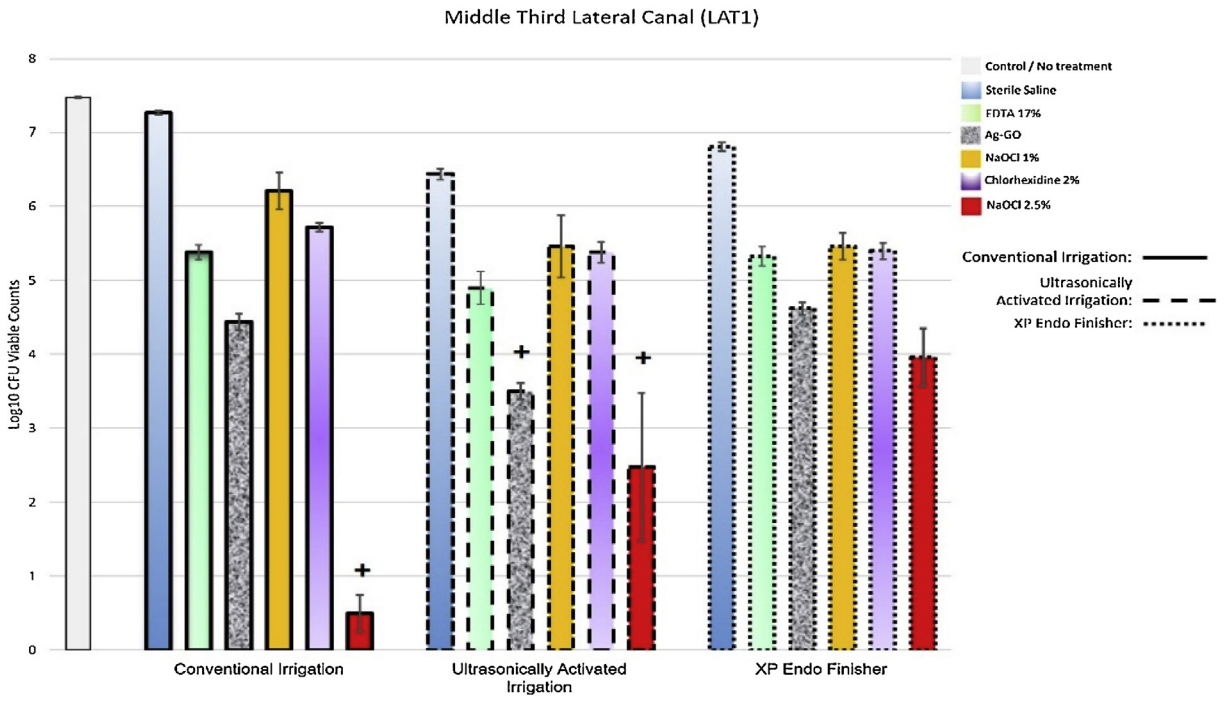


**Fig. 8 – The effect of microbial killing of root canal irrigants and agitation methods in the middle third lateral canal (LAT1). The data are expressed as mean(SD) detectable anaerobic quantitative viable counts ($log_{10}$CFU).**
**+Values significantly less compared to rest experimental groups ($P < 0.05$).**

3.3.2. *Middle lateral canal sampling point (LAT1)*

Sterile saline, EDTA 17%, CHX 2% and NaOCl 1% presented limited microbial killing efficacy, which was not statistically different from the positive control group ($P > 0.05$) (Fig. 8).

Ag-GO (UAI) and NaOCl 2.5% (CI), (UAI) enhanced microbial killing efficacy compared to the rest of the experimental groups ($P < 0.05$) (Fig. 8).

The application of XPEF deteriorated the microbial killing efficacy of Ag-GO and NaOCl 2.5% and viable counts ($log_{10}$CFU) were not statistically different compared to sterile saline and positive control groups ($P > 0.05$) (Fig. 8).

Negative control group specimens presented non-detectable viable counts ($log_{10}$CFU).

3.3.3. *Apical lateral canal sampling point (LAT2)*

NaOCl 2.5% presented non-detectable viable counts ($log_{10}$CFU), regardless of the applied irrigant delivery method.

The application of UAI significantly improved the microbial killing efficacy of Ag-GO compared to CI and XPEF, as well as compared to NaOCl 1% (UAI), (XPEF) and CHX 2% (UAI), (XPEF) ($P < 0.05$) (Fig. 9).

Limited microbial killing efficacy was observed with the application of CHX 2% (CI), (UAI), with no statistical difference compared to sterile saline and control groups ($P > 0.05$) (Fig. 9). The application of XPEF significantly improved the performance of CHX 2% compared to CHX 2% (CI), (UAI) ($P < 0.05$) (Fig. 9). CHX 2% (XPEF), NaOCl 1% (XPEF) and Ag-GO (XPEF) did not present significant differences in their viable counts ($log_{10}$CFU) ($P > 0.05$) (Fig. 9).

All negative control group specimens presented non-detectable viable counts (log10CFU).

### 3.4. *Effects of irrigants on biofilm disruption*

The effects of irrigants and their agitation techniques on biofilm disruption, in the main and lateral canals of the tooth specimens are presented in Table 2. All treatment groups presented significantly less total biovolume compared to the positive control group (no treatment) ($P < 0.05$). The maximum biofilm disruption was achieved by NaOCl 2.5% (CI), (UAI) and no viable biovolumes were present due to absence of green or red fluorescence. With the application of XPEF, a residual biovolume was present only in middle lateral canals with a mean percentage of 32% representing red (dead) biovolume.

Ag-GO presented significant reduction of total biovolumes compared to 17% EDTA, 2% CHX and 1% NaOCl, regardless of irrigation/agitation method [(CI), (UAI), (XPEF)] ($P < 0.05$). The application of UAI enhanced its biofilm disruption capacity with a mean percentage of 57% representing red (dead) biovolume, which was statistically significant compared to CI (27% red biovolume) and XPEF (25% red biovolume) ($P < 0.05$).

The application of UAI significantly improved the disruption efficacy of EDTA 17% and NaOCl 1%, compared to CI and XPEF, respectively, as well as compared to CHX 2% (CI), (UAI), (XPEF) ($P < 0.05$). However, EDTA 17% (UAI) did not present enhanced killing activity, with a mean percentage of 86% representing green (live) biovolume. With the use of NaOCl 1% (UAI), the enhancement of biofilm disruption efficacy was associated with an increase in the mean percentage of red (dead) biovolume (38%), which was statistically significant compared to CI (16% red biovolume).

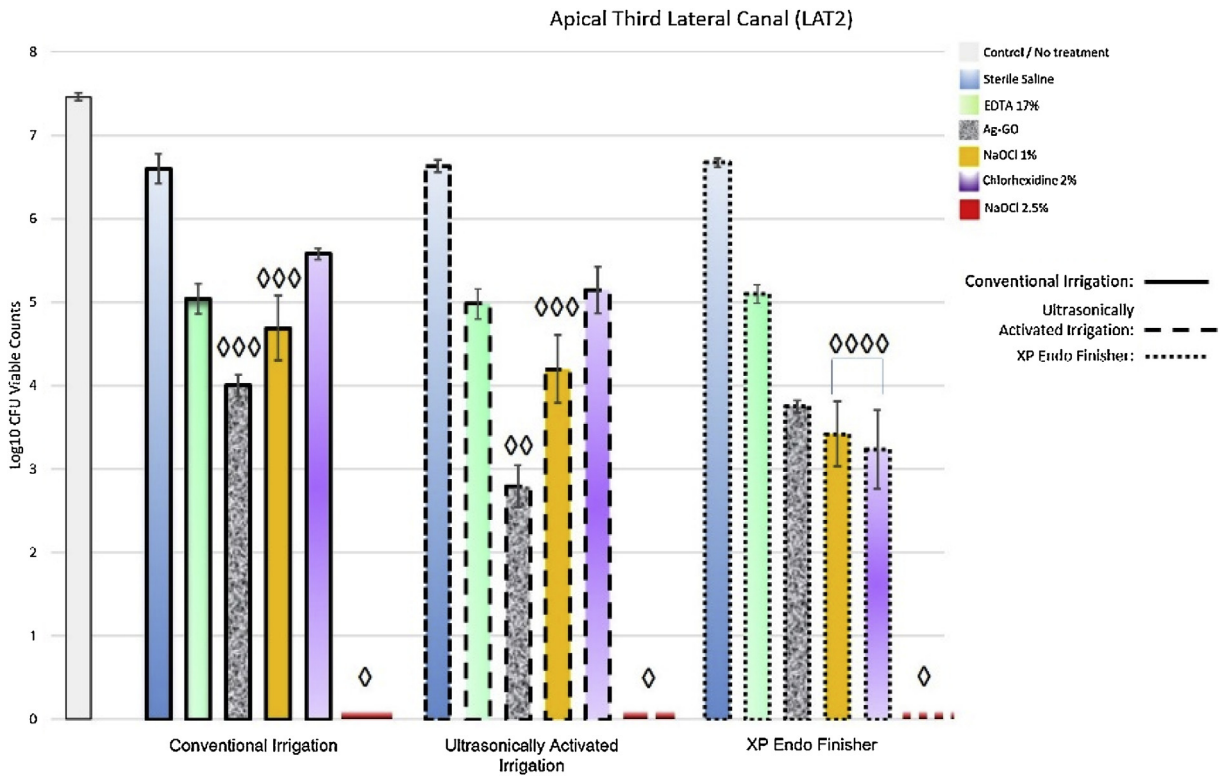


**Fig. 9 – The effect of microbial killing of root canal irrigants and agitation methods in the apical third lateral canal (LAT2). The data are expressed as mean(SD) detectable anaerobic quantitative viable counts ($log_{10}$CFU). ◊N/D: non-detectable values of anaerobic quantitative viable counts (log10CFU). ◊◊Values significantly less compared to rest experimental groups ($P < 0.05$). ◊◊◊Values significantly less compared to EDTA 17 (CI), CHX 2% (CI), EDTA 17% (UAI), CHX 2% (UAI) ($P < 0.05$). ◊◊◊◊Values significantly less compared to NaOCl 1% (CI), CHX 2% (CI), NaOCl 1% (UAI) and CHX 2% (UAI) groups ($P < 0.05$).**

## 4. Discussion

The present study showed that the use of Ag-GO under ultrasonic activation in the artificial lateral canals presented improved microbial killing efficacy compared to CI and XPEF. The antimicrobial efficacy of Ag-GO (UAI) in lateral canals was superior to that of NaOCl 1%, CHX 2%, EDTA 17% and sterile saline. In the apical third lateral canal, the use of NaOCl 2.5% (CI, UAI, XPEF) resulted in non-detectable microbial counts. An increase in NaOCl concentration and high levels of apical shear wall stress may enhance the elimination of apical lateral canal biofilm [44]. In the main canal lumen, the microbial killing efficacy of Ag-GO was similar to levels achieved with NaOCl 1% and CHX 2%. The use of CLSM further disclosed a significant reduction in total microbial biovolume on dentine surfaces, compared to all experimental groups, except NaOCl 2.5%, and regardless of irrigant delivery/activation method. The use of Ag-GO (UAI) contributed to the reduction of total microbial biovolume, as well as resulted in a high level of dead (red signal) bacteria (57%).

The use of Ag NPs has been reported to display minor biofilm disruption capacity compared to NaOCl, in root canal dentine sections examined by CLSM [45]. Previous studies also indicate that the rate of bacterial killing by nanoparticles depend on the concentration and duration of interaction [46,47]. The limited effectiveness of sole irrigation with Ag NPs is attributed to the short time period of root canal irrigation and the protective role of the biofilm matrix, making it less susceptible to antimicrobial treatments [48]. Other studies report that sole Ag NPs may not be stable in suspension to exert their antimicrobial activity due to agglomeration, resulting from the resistance of some bacteria, which can produce the adhesive flagellum protein flagellin, which triggers aggregation of the Ag NPs [49].

The multi-potent mechanism of antimicrobial action of GO has gained attention, especially as the bi-dimensional GO sheets can act as cutters of cell membranes. In particular, the sharp edges of GO can mechanically disrupt bacterial membranes leading to leakage of the intracellular cytoplasm, increase of reactive oxygen species and cell death [50–52]. GO sheets can also make a flexible web or blanket around microorganisms, envelop and wrap around the cell surfaces without penetration. This isolates them from the external environment and nutrients, leading to inactivation of proliferation and reduction in glucose consumption [53]. In addition, the antimicrobial properties of GO are also associated to its low pH values especially if GO is not subjected to purification pro-

cedures that allows soluble acidic impurities to remain within the milieu [54].

Hence the incorporation of Ag NPs within GO sheets to form an aqueous Ag-GO suspension was tested for the first time for root canal disinfection using a nutrient-stressed, multi-species biofilm developed in an infected tooth model, *ex vivo*. The mechanism of Ag-GO formation has been attributed to the presence of oxygenic functional groups, such as hydroxyl, epoxide and carboxyl, on the GO, which provide a large number of binding sites for Ag ions [55]. Following the *in situ* reduction by $NaBH_4$ in aqueous solution, the positively charged $Ag^+$ ions can be easily captured by negatively charged GO surface through physicosorption, electrostatic binding and charge-transfer interactions [56]. The hybrid material of Ag NPs within a matrix of a layered material like GO can induce binding capability, which is usually lacking in Ag NPs alone, and enhance its synergistic antimicrobial activity compared to sole GO or Ag NPs [57]. Thus, a stable Ag-GO nanocomposite was formed to overcome aggregation and stability.

A new *ex vivo* tooth model was developed in order to improve stability and retention of hemi-sected root specimens and minimise the effect of thickness reduction, with use of a microtome. The model was reproducible and allowed for the simulation of an *ex vivo* closed apical system, to partially overcome methodological limitations from the absence of periradicular tissue pressure [37]. All tested irrigants were subjected to challenging environmental conditions, associated with no instrumentation but direct exposure against the biofilm, application of limited irrigant volume, low flow rate, as well as short exposure time. This was decided with a view to assess the effect of irrigant delivery and activation methods and reduce the carry-over antimicrobial effect of concentrated solutions.

Sterile saline had no effect on microbial killing. Although a significant reduction in total biovolume was observed compared to positive control group under CLSM, no difference was found in live (green) biofilm viability. This finding suggests that microbial killing cannot be achieved with agitation methods only; thus, the use of a chemical active disinfectant is essential [11,35]. As a chelating agent, EDTA 17% can bind calcium ions, which are essential for cell co-adherence and stabilization of extracellular polymeric substance of a biofilm [58,59]. Thus, the moderate biofilm disruption observed on application of UAI can be attributed to its biofilm-dispersing properties [23]. The role of EDTA in biofilm detachment and root canal cleaning has not been elucidated yet and requires further investigation.

Several studies have shown that compared to conventional irrigation, the application of UAI or XPEF enhances the efficacy of NaOCl in reducing intra-canal bacteria and removing biofilms from the main canal lumen, the apical third root surface and shallow or deep layers of root dentine [60,61]. In this study, the application of UAI or XPEF did not improve microbial killing compared to conventional syringe irrigation, when Ag-GO, CHX 2% and NaOCl 1% or 2.5% were used. The differ-

**Table 2 – The effect of irrigation and agitation methods on biofilm disruption. The results represented the remaining mean (SE) values of total biovolume ($\mu m^3/\mu m^2$) and their respective mean percentages of dead (red), live (green) and unknown (orange) microbial populations. Representative confocal images of residual biofilms from the 3 examined areas are also presented (for interpretation of the references to colour in this table legend, the reader is referred to the web version of this article).**

| Irrigant type | Irrigation Activation method | Total biovolume ($um^3/um^2$) Mean(se) | Percentage mean of total biovolume Green: Live Red: Dead Orange: unknown | Location within root canal system | | |
|---|---|---|---|---|---|---|
| | | | | Main root canal (apical third) | Middle lateral canal | Apical lateral canal |
| Positive control | No treatment | 300369 (128447) [a] | 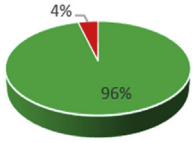  | 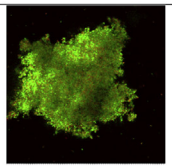 | 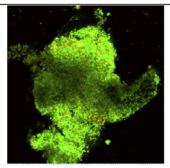 | 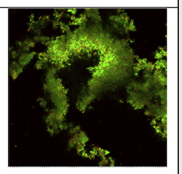 |
| Sterile Saline | CI | 180221 (104961) | 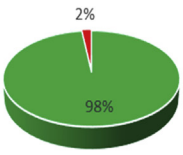  | 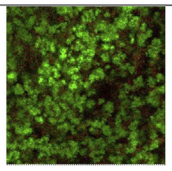 | 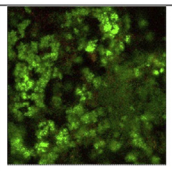 | 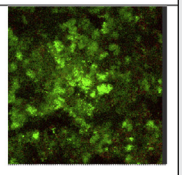 |
| | UAI | 212291 (32532) | 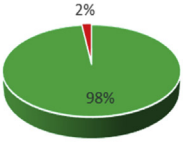  | 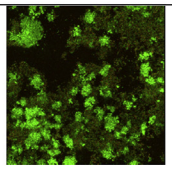 | 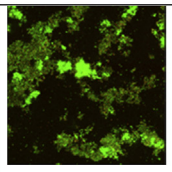 | 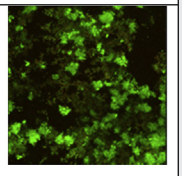 |

**Table 1 (*Continued*)**

| | | | | | | |
|---|---|---|---|---|---|---|
| | XPEF | 218844 (43284) | 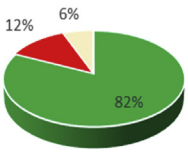 | 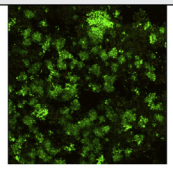 | 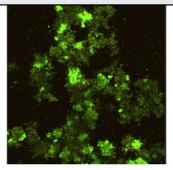 | 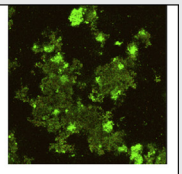 |
| EDTA 17% | CI | 125175 (88862) | 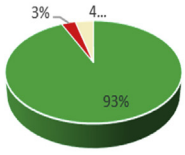 | 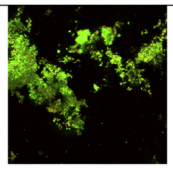 | 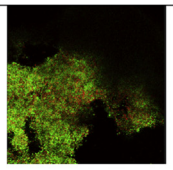 | 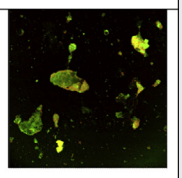 |
| | UAI | 60582 (27376) [b] | 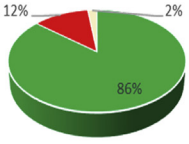 | 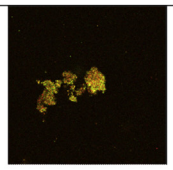 | 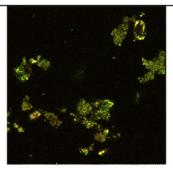 | 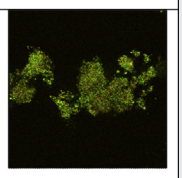 |
| | XPEF | 164373 (22490) | 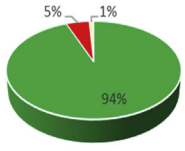 | 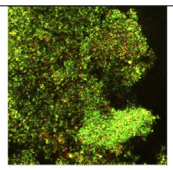 | 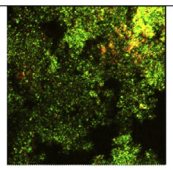 | 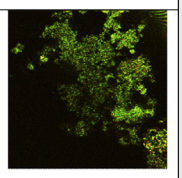 |
| CHX 2% | CI | 104710 (13275) | 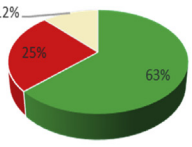 | 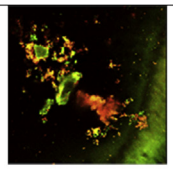 | 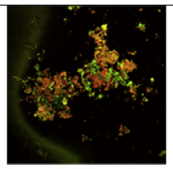 | 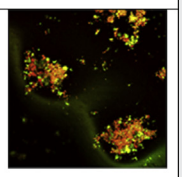 |
| | UAI | 128888 (44671) | 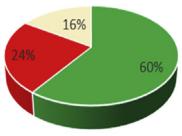 | 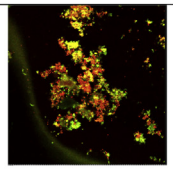 | 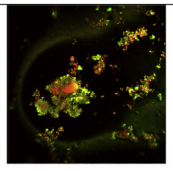 | 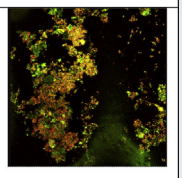 |
| | XPEF | 133646 (53546) | 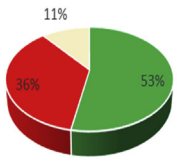 | 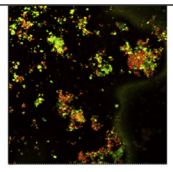 | 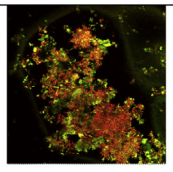 | 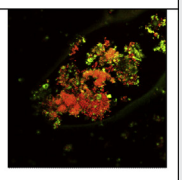 |

**Table 1 (*Continued*)**

| | | | | | | |
|---|---|---|---|---|---|---|
| NaOCl 1% | CI | 107791 (73570) | 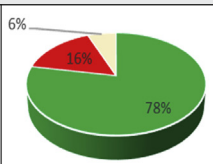 | 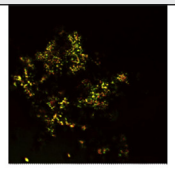 | 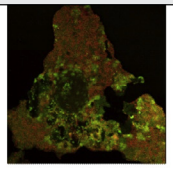 | 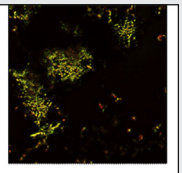 |
| | UAI | 45670 (29459) [c] | 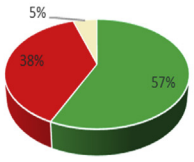 | 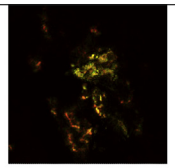 | 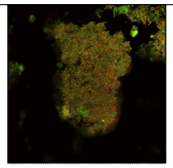 | 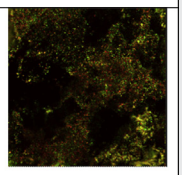 |
| | XPEF | 180431 (131649) | 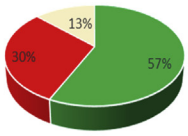 | 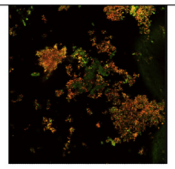 | 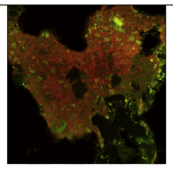 | 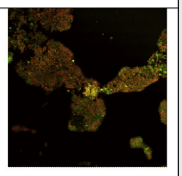 |
| Ag-GO | CI | 26182 (8374) [d] | 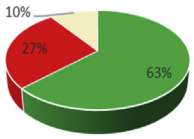 | 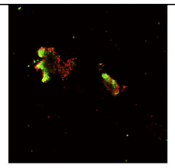 | 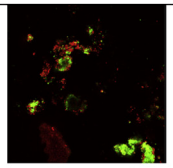 | 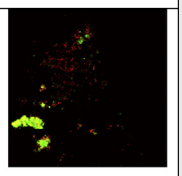 |
| | UAI | 17272 (7050) [d,e] | 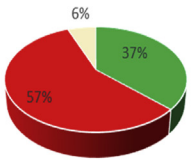 | 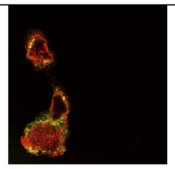 | 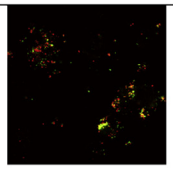 | 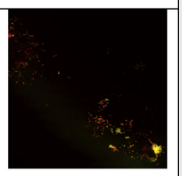 |
| | XPEF | 22283 (7296) [d] | 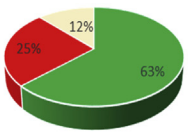 | 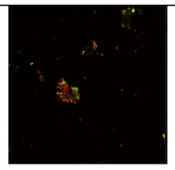 | 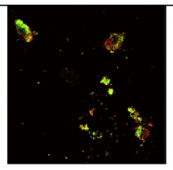 | 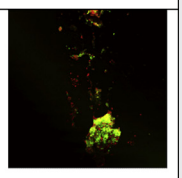 |
| NaOCl 2.5% | CI | N/D | 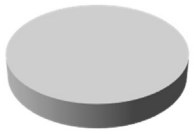 |  |  | 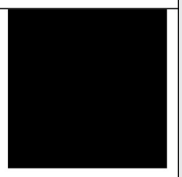 |
| | UAI | N/D | 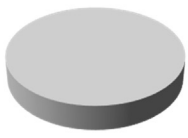 |  |  | 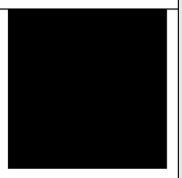 |

**Table 1 (*Continued*)**

| | | | | | | |
|---|---|---|---|---|---|---|
| | XPEF | 152583 (50861) *Detectable in middle root lateral canal | 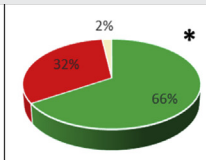  |  | 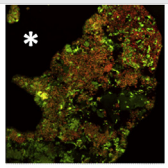  |  |

[a]Mean (SE) total biovolume values significantly higher compared to all experimental groups ($P < 0.05$).
[b]Mean (SE) total biovolume values from the use of EDTA 17% (UAI) significantly less compared to EDTA 17% (CI), (XPEF) ($P < 0.05$).
[c]Mean (SE) total biovolume values from the use of NaOCl 1% (UAI) significantly less compared to NaOCl 1% (CI), (XPEF) ($P < 0.05$).
[d]Mean (SE) total biovolume values from the use of Ag-GO (CI), (UAI), (XPEF) significantly less compared to their respective in EDTA 17%, CHX 2% and NaOCl groups ($P < 0.05$).
[e]Mean (SE) total biovolume values from the use of Ag-GO (UAI) significantly less compared to Ag-GO (CI), (XPEF) ($P < 0.05$).

ences can be attributed to different methodologies, irrigant concentrations and volume as well as total time/flow rate.

In single rooted teeth, lateral canals branch from the main root canal, have narrow orifices with diameters typically ranging from 10 to 400 μm [62], that create a surface tension barrier, which limits adequate mixing of irrigant with the fluid within it [63]. To the authors' best knowledge, this is the first *ex vivo* tooth model, in which, the artificially prepared canals were characterised and quantified by using NCLP, ensuring the consistency of their dimensions. The use of 3D step height to quantify z-dimensional data, according to ISO 5436-1, has been previously described as an appropriate method for quantifying step-heights and valleys, which is what these artificial lateral canals can be classified as, within the context of surface metrology [36]. Thus, the efficacy of irrigation was evaluated in standardized apical and middle root third artificial lateral canals.

The antimicrobial efficacy of Ag-GO (UAI) was superior to that of NaOCl 1%, CHX 2%, EDTA 17% and sterile saline, in the apical third lateral canal. The use of XPEF did not improve the microbial killing efficacy of Ag-GO compared to UAI, but improved the performance of NaOCl 1% and CHX 2%. Our results are in agreement with a previous study, in which XPEF was found to be more effective compared to UAI and CI in removing biofilms from artificial apical lateral grooves [64]. However, the exact mode of action of XPEF on irrigant delivery across a shaped root canal system needs further investigation.

The biofilm in middle root third lateral canal was least affected by the irrigants and the agitation methods used had limited effects, when NaOCl 1% (CI, UAI, XPEF), CHX 2% (CI, UAI, XPEF) and NaOCl 2.5% (XPEF) were used. This finding may be related to several parameters arising due to the dynamic conditions, which exist coronally to the insertion depth of the irrigation needle. This results in reduction of shear wall stress, leading to limited contact of irrigant with biofilm layer; low velocity of irrigant exchange with an absence of developing jet are also associated with the limited antimicrobial performance in middle lateral canal [14,65]. Finally, the increased length of a lateral canal in the middle root third combined with limited irrigant penetration may further predispose for poor disinfection outcomes.

A significant reduction in the microbial counts of the middle root third lateral canal was observed with NaOCl 2.5% (CI), (UAI) whilst Ag-GO (UAI) exhibited equivalence to NaOCl 2.5% (UAI) and superior efficacy compared to the rest of the experimental groups. These findings can be attributed to a potentially existing, dual and synergistic mechanism of action of Ag-GO. The increased formation of reactive oxygen species has the ability to react with various biomacromolecules, causing irreversible oxidative damage, loss of cellular DNA replication ability and cell death [66]. The enhancement of Ag-GO microbial killing and biofilm disruption efficacy with the use of UAI may correlate to a substantial increase in the velocity of the Ag-GO nanosheets against the exposed biofilm layers and cause an increase in temperature, which may enhance the kinetics of the Ag-GO nanosheets on a molecular level. The significant reduction in biofilm biovolume may also result from the wrapping capacity of Ag-GO sheets around ruptured biofilms and their detachment from dentinal tubules [67], with the aid of the developing jet when UAI is applied.

The application of Ag-GO for root canal irrigation as an alternative to NaOCl has potential, however studies are required to further elucidate the mechanism of action against endodontic biofilms. Ag-GO can be implemented as auxiliary disinfectant in cases of NaOCl intolerance as well as cases where a high risk of irrigant extrusion is present. This may apply to infected roots with incomplete development, open root apices affected by external inflammatory apical root resorption, close proximity of root apices to maxillary sinus, as well as the mental or inferior dento-alveolar nerve. Ag-GO presents low cytotoxicity and high biocompatibility [68,69] and potentially can be used as a platform for the safe delivery of inter-appointment antimicrobial medicaments.

## 5. Conclusion

Within the limitations of this study, the microbial killing and biofilm disruption capacity of Ag-GO was successfully achieved using a novel *ex vivo* infected tooth model. The efficacy of irrigation protocols was affected by the sampling point areas of the infected root canal model. NaOCl 2.5% presented superior antimicrobial efficacy at all sampling sites and it was found that the middle root third lateral canal was the least affected sampling point area. Ultrasonic activation selectively

enhanced the microbial killing and biofilm disruption of Ag-GO in lateral canals.

## REFERENCES


[1] Costerton JW, Stewart PS, Greenberg EP. Bacterial biofilms: a common cause of persistent infections. Science 1999;284:1318–22.
[2] Kakehashi S, Stanley H, Fitzgerald R. The effect of surgical exposures of dental pulps in germ-free and conventional laboratory rats. Oral Surg Oral Med Oral Pathol 1965;20:340–9.
[3] Möller AJ, Fabricius L, Dahlén G, Ohman AE, Heyden G. Influence on periapical tissues of indigenous oral bacteria and necrotic pulp tissue in monkeys. Scand J Dent Res 1981;89:475–84.
[4] Donlan RM. Biofilms: microbial life on surfaces. Emerg Infect Dis 2002;8:881–90.
[5] Costerton W, Veeh R, Shirtliff M, Pasmore M, Post C, Ehrlich G. The application of biofilm science to the study and control of chronic bacterial infections. J Clin Invest 2003;112:1466–77.
[6] Peters OA, Boessler C, Paqué F. Root canal preparation with a novel nickel-titanium instrument evaluated with micro-computed tomography: canal surface preparation over time. J Endod 2010;36:1068–72.
[7] Love RM. *Enterococcus faecalis*: a mechanism for its role in endodontic failure. Int Endod J 2001;34:399–405.
[8] Nair PNR. Pathogenesis of apical periodontitis and the causes of endodontic failures. Crit Rev Oral Biol Med 2004;15:348–81.
[9] Ricucci D, Loghin S, Siqueira Jr JF. Exuberant Biofilm infection in a lateral canal as the cause of short-term endodontic treatment failure: report of a case. J Endod 2013;39:712–8.
[10] Sedgley C. Root canal irrigation—a historical perspective. J Hist Dent 2004;52:61–5.
[11] Siqueira Jr JF, Rôças IN, Favieri A, Lima KC. Chemomechanical reduction of the bacterial population in the root canal after instrumentation and irrigation with 1%, 2.5%, and 5.25% sodium hypochlorite. J Endod 2000;26:331–4.
[12] Clarkson RM, Moule AJ, Podlich H, Kellaway R, Macfarlane R, Lewis D, et al. Dissolution of porcine incisor pulps in sodium hypochlorite solutions of varying compositions and concentrations. Aust Dent J 2006;51:245–51.
[13] Buttler TK, Crawford JJ. The detoxifying effect of varying concentrations of sodium hypochlorite on endotoxins. J Endod 1982;8:59–66.
[14] Macedo R, Robinson J, Verhaagen B, Walmsley A, Versluis M, Cooper P, et al. A novel methodology providing insights into removal of biofilm-mimicking hydrogel from lateral morphological features of the root canal during irrigation procedures. Int Endod J 2014;47:1040–51.
[15] Gu LS, Kim JR, Ling J, Choi KK, Pashley DH, Tay FR. Review of contemporary irrigant agitation techniques and devices. J Endod 2009;35:791–804.
[16] Trope M, Debelian G. XP-3D finisher file-the next step in restorative endodontics. Endod Pract 2015;8:22–4.
[17] Oyarzún A, Cordero AM, Whittle M. Immunohistochemical evaluation of the effects of sodium hypochlorite on dentin collagen and glycosaminoglycans. J Endod 2002;28:152–6.
[18] Pashley EL, Birdsong NL, Bowman K, Pashley DH. Cytotoxic effects of NaOCl on vital tissue. J Endod 1985;11:525–8.
[19] Kerbl FM, DeVilliers P, Litaker M, Eleazer PD. Physical effects of sodium hypochlorite on bone: an ex vivo study. J Endod 2012;38:357–9.
[20] Varise TG, Estrela C, Costa Guedes DF, Sousa-Neto MD, Pécora JD. Detection of organochlorine compounds formed during the contact of sodium hypochlorite with dentin and dental pulp. Braz Dent J 2014;25:109–16.
[21] Ioannidis K, Niazi S, Deb S, Mannocci F, Smith D, Turner C. Quantification by SIFT-MS of volatile compounds produced by the action of sodium hypochlorite on a model system of infected root canal content. PLoS One 2018;13:e0198649.
[22] Naenni N, Thoma K, Zehnder M. Soft tissue dissolution capacity of currently used and potential endodontic irrigants. J Endod 2004;30:785–7.
[23] de Almeida J, Hoogenkamp M, Felippe WT, Crielaard W, van der Waal SV. Effectiveness of EDTA and modified salt solution to detach and kill cells from *Enterococcus faecalis* biofilm. J Endod 2016;42:320–3.
[24] Bassegoda A, Ivanova K, Ramon E, Tzanov T. Strategies to prevent the occurrence of resistance against antibiotics by using advanced materials. Appl Microbiol Biotechnol 2018;102:2075–89.
[25] Choi O, Deng KK, Kim NJ, Ross Jr L, Surampalli RY, Hu Z. The inhibitory effects of silver nanoparticles, silver ions, and silver chloride colloids on microbial growth. Water Res 2008;42:3066–74.
[26] Rai M, Yadav A, Gade A. Silver nanoparticles as a new generation of antimicrobials. Biotechnol Adv 2009;27:76–83.
[27] Geim AK, Novoselov KS. The rise of graphene. Nat Mater 2007;6:183–91.
[28] Li D, Muller MB, Gilje S, Kaner RB, Wallance GG. Processable aqueous dispersions of graphene nanosheets. Nat Nanotechnol 2008;3:101–5.
[29] Serrano-Aroca Á, Deb S. Synthesis of irregular graphene oxide tubes using green chemistry and their potential use as reinforcement materials for biomedical applications. PLoS One 2017;12:e0185235.
[30] Tu Y, Lv M, Xiu P, Huynh T, Zhang M, Castelli M, et al. Destructive extraction of phospholipids from *Escherichia coli* membranes by graphene nanosheets. Nat Nanotechnol 2013;8:594–601.
[31] He J, Zhu X, Qi Z, Wang C, Mao X, Zhu C, et al. Killing dental pathogens using antibacterial graphene oxide. ACS Appl Mater Interfaces 2015;7:5605–11.
[32] Chung C, Kim YK, Shin D, Ryoo SR, Hong BH, Min DH. Biomedical applications of graphene and graphene oxide. Acc Chem Res 2013;46:2211–24.
[33] Das MR, Sarma RK, Saikia R, Kale VS, Shelke MV, Sengupta P. Synthesis of silver nanoparticles in an aqueous suspension of graphene oxide sheets and its antimicrobial activity. Colloids Surf B: Biointerfaces 2011;83:16–22.
[34] Song B, Zhang C, Zeng G, Gong J, Chang Y, Jiang Y. Antibacterial properties and mechanism of graphene oxide-silver nanocomposites as bactericidal agents for water disinfection. Arch Biochem Biophys 2016;604:167–76.
[35] Niazi SA, Clark D, Do T, Gilbert SC, Foschi F, Mannocci F, et al. The effectiveness of enzymic irrigation in removing a nutrient-stressed endodontic multispecies biofilm. Int Endod J 2014;47:756–68.
[36] Mylonas P, Austin RS, Moazzez R, Joiner A, Bartlett DW. In vitro evaluation of the early erosive lesion in polished and natural human enamel. Dent Mater 2018;34:1391–400.
[37] Psimma Z, Boutsioukis C, Vasiliadis L, Kastrinakis E. A new method for real-time quantification of irrigant extrusion during root canal irrigation ex vivo. Int Endod J 2013;46:619–31.
[38] Dahlén G, Konradsson K, Eriksson S, Teanpaisan R, Piwat S, Carlén A. A microbiological study in relation to the presence of caries and calculus. Acta Odontol Scand 2010;68:199–206.
[39] Niazi SA, Clarke D, Do T, Gilbert SC, Mannocci F, Beighton D. *Propionibacterium acnes* and *Staphylococcus epidermidis* isolated from refractory endodontic lesions are opportunistic pathogens. J Clin Microbiol 2010;48:3859–69.

[40] Gmür R, Guggenheim B. Antigenic heterogeneity of *Bacteroides intermedius* as recognized by monoclonal antibodies. Infect Immun 1983;42:459–70.
[41] Shu R, Yin Q, Xing H, Tan D, Gan Y, Xu G. Colloidal and rheological behavior of aqueous graphene oxide dispersions in the presence of poly(ethylene glycol). Colloids Surf A: Physicochem Eng Asp 2016;488:154–61.
[42] Vogel AI. A text-book of quantitative inorganic analysis. 1st ed. London: Longman; 1962.
[43] Chávez de Paz LE. Image analysis software based on color segmentation for characterization of viability and physiological activity of biofilms. Appl Environ Microbiol 2009;75:1734–9.
[44] Layton G, Wu WI, Selvaganapathy PR, Friedman S, Kishen A. Fluid dynamics and biofilm removal generated by syringe-delivered and 2 ultrasonic-assisted irrigation methods: a novel experimental approach. J Endod 2015;41:884–9.
[45] Wu D, Fan W, Kishen A, Gutmann JL, Fan B. Antibiofilm efficacy of silver nanoparticles as a vehicle for calcium hydroxide medicament against *Enterococcus faecalis*. J Dent 2015;43:1573–9.
[46] Kishen A, Shi Z, Shrestha A, Neoh KG. An investigation on the antibacterial and antibiofilm efficacy of cationic nanoparticulates for root canal disinfection. J Endod 2008;34:1515–20.
[47] Shrestha A, Shi Z, Neoh KG, Kishen A. Nanoparticulates for antibiofilm treatment and effect of aging on its antibacterial activity. J Endod 2010;36:1030–5.
[48] Rodrigues CT, de Andrade FB, de Vasconcelos LRSM, Midena RZ, Pereira TC, Kuga MC, et al. Antibacterial properties of silver nanoparticles as a root canal irrigant against *Enterococcus faecalis* biofilm and infected dentinal tubules. Int Endod J 2018;51:901–11.
[49] Panacek A, Kvitek L, Smekalova M, Vecerova R, Kolar M, Roderova M, et al. Nat Nanotechnol 2018;13:65–71.
[50] Akhavan O, Ghaderi E. Toxicity of graphene and graphene oxide nanowalls against bacteria. ACS Nano 2010;4:5731–6.
[51] Liu S, Zeng TH, Hofmann M, Burcombe E, Wei J, Jiang R, et al. Antibacterial activity of graphite, graphite oxide, graphene oxide, and reduced graphene oxide: membrane and oxidative stress. ACS Nano 2011;5:6971–80.
[52] Combarros R, Collado S, Díaz M. Toxicity of graphene oxide on growth and metabolism of *Pseudomonas putida*. J Hazard Mater 2016;310:246–52.
[53] Akhavan O, Ghaderi E, Esfandiar A. Wrapping bacteria by graphene nanosheets for isolation from environment, reactivation by sonication, and inactivation by near-infrared irradiation. J Phys Chem B 2011;115:6279–88.
[54] Barbolina I, Woods CR, Lozano N, Kostarelos K, Novoselov KS, Roberts IS. Purity of graphene oxide determines its antibacterial activity. 2D Mater 2016;3:025025.
[55] Zhu Z, Su M, Ma L, Liu D, Wang Z. Preparation of graphene oxide silver nanoparticle nanohybrids with highly antibacterial capability. Talanta 2013;117:449–55.
[56] Hui KS, Hui KN, Dinh DA, Tsang CH, Cho YR, Zhou W, et al. Green synthesis of dimension-controlled silver nanoparticle-graphene oxide with in situ ultrasonication. Acta Mater 2014;64:326–32.
[57] Liu S, Cao S, Guo J, Luo L, Zhou Y, Lin C, et al. Graphene oxide-silver nanocomposites modulate biofilm formation and extracellular polymeric substance (EPS) production. Nanoscale 2018;10:19603–11.
[58] Chen X, Stewart PS. Biofilm removal caused by chemical treatments. Water Res 2000;34:4229–33.
[59] Chávez de Paz LE, Bergenholtz G, Svensäter G. The effects of antimicrobials on endodontic biofilm bacteria. J Endod 2010;36:70–7.
[60] Alves FR, Andrade-Junior CV, Marceliano-Alves MF, Pérez AR, Rôças IN, Versiani MA, et al. Adjunctive steps for disinfection of the mandibular molar root canal system: a correlative bacteriologic, micro-computed tomography, and cryopulverization approach. J Endod 2016;42:1667–72.
[61] Azim AA, Aksel H, Zhuang T, Mashtare T, Babu JP, Huang GT. Efficacy of 4 irrigation protocols in killing bacteria colonized in dentinal tubules examined by a novel confocal laser scanning microscope analysis. J Endod 2016;42:928–34.
[62] Miyashita M, Kasahara E, Yasuda E, Yamamoto A, Sekizawa T. Root canal system of the mandibular incisor. J Endod 1997;23:479–84.
[63] Wang R, Shen Y, Ma J, Huang D, Zhou X, Gao Y, et al. Evaluation of the effect of needle position on irrigant flow in the C-shaped root canal using a computational fluid dynamics model. J Endod 2015;41:931–6.
[64] Bao P, Shen Y, Lin J, Haapasalo M. In vitro efficacy of XP-endo finisher with 2 different protocols on biofilm removal from apical root canals. J Endod 2017;43:321–5.
[65] Robinson JP, Macedo RG, Verhaagen B, Versluis M, Cooper PR, van der Sluis LWM, et al. Cleaning lateral morphological features of the root canal: the role of streaming and cavitation. Int Endod J 2018;51:e55–64.
[66] Feng QL, Wu J, Chen GQ, Cui FZ, Kim TN, Kim JO. A mechanistic study of the antibacterial effect of silver ions on *Escherichia coli* and *Staphylococcus aureus*. J Biomed Mater Res 2000;52:662–8.
[67] Afkhami F, Pourhashemi SJ, Sadegh M, Salehi Y, Fard MJ. Wrapping bacteria by graphene nanosheets for isolation from environment, reactivation by sonication, and inactivation by near-infrared irradiation. J Phys Chem B 2011;115:6279–88.
[68] Cai X, Tan S, Yu A, Zhang J, Liu J, Mai W, et al. Sodium 1-naphthalenesulfonate-functionalized reduced graphene oxide stabilizes silver nanoparticles with lower cytotoxicity and long-term antibacterial activity. Chem Asian J 2012;7:1664–70.
[69] Zhang P, Wang H, Zhang X, Xu W, Li Y, Li Q, et al. Graphene film doped with silver nanoparticles: self-assembly formation, structural characterizations, antibacterial ability, and biocompatibility. Biomater Sci 2015;3:852–60.